Structure

H95 Is a pH-Dependent Gate in Aquaporin 4

Highlights

- AQP4 is studied using combined molecular dynamics and in vitro studies

- Regulation of the permeability of AQP4 is shown to be pH sensitive

- The protonation state of H95 is shown to influence the permeability of the protein

- The H95A mutant loses pH sensitivity

Authors

Shreyas Kaptan, Mette Assentoft, Hans Peter Schneider, Robert A. Fenton, Joachim W. Deitmer, Nanna MacAulay, Bert L. de Groot

Correspondence

bgroot@gwdg.de

In Brief

Kaptan et al. demonstrate that AQP4 permeability is regulated via a conserved histidine residue H95. The regulation is dependent on the protonation state of the residue and is sensitive to cytoplasmic pH conditions. A mutation of H95 to alanine abolishes the pH sensitivity of AQP4.

CrossMark

CellPress

H95 Is a pH-Dependent Gate in Aquaporin 4

Shreyas Kaptan,[1] Mette Assentoft,[2] Hans Peter Schneider,[3] Robert A. Fenton,[4] Joachim W. Deitmer,[3] Nanna MacAulay,[2] and Bert L. de Groot[1,*]

[1]Computational Biomolecular Dynamics Group, Max Planck Institute for Biophysical Chemistry, Am Fassberg 11, 37077 Göttingen, Germany
[2]Department of Cellular and Molecular Medicine, Faculty of Health and Medical Sciences, The Panum Institute, Blegdamsvej 3, 2200 Copenhagen N, Denmark
[3]Division of General Zoology, Department of Biology, University of Kaiserslautern, 67653 Kaiserslautern, Germany
[4]Department of Biomedicine, InterPrET Center, Aarhus University, Nordre Ringgade 1, 8000 Aarhus C, Denmark
*Correspondence: bgroot@gwdg.de
http://dx.doi.org/10.1016/j.str.2015.08.020

SUMMARY

Aquaporin 4 (AQP4) is a transmembrane protein from the aquaporin family and is the predominant water channel in the mammalian brain. The regulation of permeability of this protein could be of potential therapeutic use to treat various forms of damage to the nervous tissue. In this work, based on data obtained from in silico and in vitro studies, a pH sensitivity that regulates the osmotic water permeability of AQP4 is demonstrated. The results indicate that AQP4 has increased water permeability at conditions of low pH in atomistic computer simulations and experiments carried out on *Xenopus* oocytes expressing AQP4. With molecular dynamics simulations, this effect was traced to a histidine residue (H95) located in the cytoplasmic lumen of AQP4. A mutant form of AQP4, in which H95 was replaced with an alanine (H95A), loses sensitivity to cytoplasmic pH changes in in vitro osmotic water permeability, thereby substantiating the in silico work.

INTRODUCTION

Aquaporins are involved in handling the permeation of water across cell membranes (Agre, 2006; Agre et al., 2002). Each of the monomers in this tetrameric transmembrane protein acts as a channel through which bidirectional osmotic water transport takes place between the extracellular space and cytoplasmic compartment (Meinild et al., 1998). The three-dimensional structure of these proteins is highly conserved, with each monomer accommodating an hourglass-shaped pore. The narrowest restriction is characterized by a highly conserved arginine residue in a hydrophobic environment, being labeled as aromatic/arginine (ar/R) region. Another conserved feature in the sequence of aquaporins is the NPA-duplex motif, placed in the interior of the pore (Murata et al., 2000). Aquaporin proteins show high specificity toward permeants, with the ability to distinguish between water molecules from protons, prohibiting the permeation of the latter (de Groot et al., 2003). Thirteen members of the aquaporin water channel family have been identified in humans (Heymann and Engel,

1999). Although most of these serve explicitly as water channels, a few permeate alternative substrates such as glycerol and urea (Beitz et al., 2004). It has been suggested that aquaporins may also serve as facilitators of gas transport, permeating small hydrophobic molecules such as ammonia, oxygen, nitrous oxide, and carbon dioxide (Agre, 2006; Cooper et al., 2002; Endeward et al., 2006; Verkman, 2002; Wang and Tajkhorshid, 2010; Zador et al., 2009).

Recently, analyses by X-ray crystallographic methods have elucidated the structural and topological features of several members of the aquaporin family of proteins: AQP1 (Murata et al., 2000; Sui et al., 2001), GlpF (Fu et al., 2000), AQPZ (Savage et al., 2003), AQP0 (Harries et al., 2004), AQYM (Lee et al., 2005), SoPIP2;1 (Törnroth-Horsefield et al., 2006), PfAQP (Newby et al., 2008), AQP5 (Horsefield et al., 2008), AQP4 (Ho et al., 2009), and AQP2 (Frick et al., 2014). These structures have provided us with insights into the inner working of the channel. Computer simulations performed with these structures as starting points further expanded our knowledge concerning the dynamic nature of the underlying molecular mechanisms. The regulation of the permeability of aquaporins has been studied extensively with molecular dynamics (MD) simulations (Burykin and Warshel, 2004; de Groot et al., 2003; de Groot and Grubmüller, 2001, 2005; Hub and de Groot, 2008; Hub et al., 2009; Lin et al., 2006; Törnroth-Horsefield et al., 2006; Yu et al., 2006), which have helped decipher mechanisms underlying physiological events that alter the choice of permeants and the rate at which these permeants diffuse through the channel.

AQP4 is the main water channel in the brain and is abundant at the perivascular glial endfeet (Amiry-Moghaddam and Ottersen, 2003; Nielsen et al., 1997). Due to its location at the blood-brain barrier and the altered survival rate of AQP4 knockout mice following experimentally inflicted brain edema formation, AQP4 has been proposed to be involved in ischemic brain edema (reviewed by Zador et al., 2009). Short-term regulation of AQP4 under pathophysiological conditions promoting brain edema has therefore attracted scientific interest. During cerebral ischemia, the pH decreases in the extracellular space and in the astrocytic cytoplasm (Beppu et al., 2014; Kraig and Chesler, 1990; Lascola and Kraig, 1997; Ringel et al., 2000). These changes in the brain environment are likely to be involved in the pathogenesis of brain ischemia and the subsequent brain edema (Beppu et al., 2014). However, the effect of these pH changes on AQP4-mediated water permeability remains to be determined. Earlier work has suggested that AQP4 is subject to regulation through covalent and
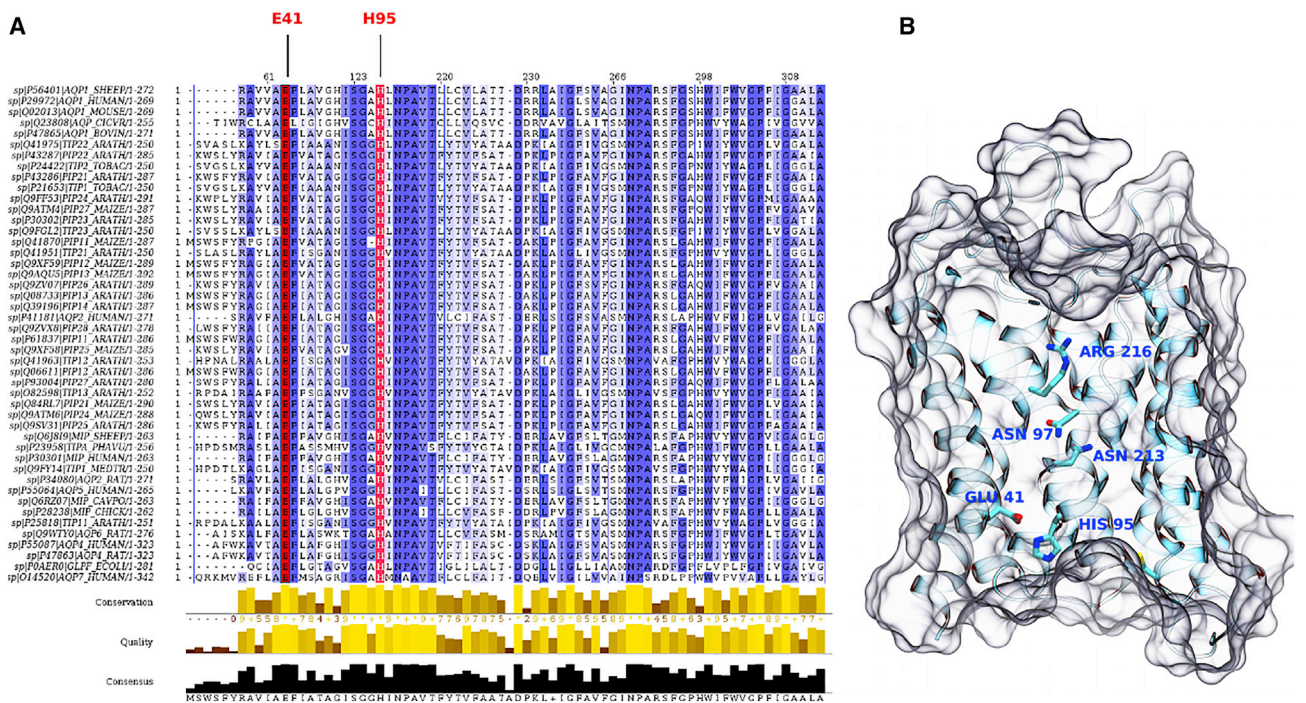
Figure 1. Conserved Residues in AQP4

(A) Sequence comparison for the protein sequences of the aquaporin family. The evolutionary conservation of the H95 residue as well as the E41 residue in the human AQP4 is highlighted in red.

(B) The conserved residues in AQP4 are shown in licorice representation.

non-covalent modification. The role of phosphorylation in regulating the localization or trafficking of AQP4 to the plasma membrane is controversial. Initial studies suggested that the two conserved serine residues S180 and S111 are targets for phosphorylation and were required for kinase-dependent gating of AQP4 (Gunnarson et al., 2008; Zelenina et al., 2002), whereas recent experimental and computational work indicated that phosphorylation of these (and a range of other) residues was not a required event for channel opening or correct targeting to the plasma membrane (Assentoft et al., 2013; Sachdeva and Singh, 2014b, Assentoft et al., 2014). AQP4 water permeability has been studied in detail with computational MD techniques (Cui and Bastien, 2011; Ho et al., 2009; Sachdeva and Singh, 2014a). An external electric field can also modulate the permeability of AQP4 by gating the H201 residue in the protein (Garate et al., 2011; Reale et al., 2013), although the water permeability of AQP4-expressing oocytes was independent of membrane potentials in the physiological range (Fenton et al., 2010). There have been computational studies to show that the solute preference of AQP4 extends beyond water to other substrates such as NO, CO_2, and O_2 (Wang and Tajkhorshid, 2010). Only recently a histidine residue, H95, has been shown to participate in a gating mechanism that could possibly be regulated by pH (Alberga et al., 2014). However, the mechanism of modulation of the permeability via pH remains unresolved. In the present work we demonstrate that AQP4 can be regulated by intracellular pH through a change in protonation of H95, and elucidate the molecular mechanisms of this effect with MD simulation and mutational analysis of heterologous expressed AQP4.

RESULTS

In our previous work (Assentoft et al., 2013), we observed that the individual monomers of AQP4 showed distinct osmotic water permeabilities that were consistent over a long time scale. We visually identified H95 moving in and out of the channel pore as a possible cause of these variations. These variations were present in both the phosphorylated and the non-phosphorylated AQP4 simulations. H95 is located in the pore of AQP4 and is conserved within plant, humans, rats, and mice (Figures 1A and B), suggesting an important role for this specific residue. To estimate the effect of the change in protonation state of H95 on AQP4 permeability with MD simulations, we performed two 500-ns equilibrium runs, with one having H95 in all four monomers in a singly protonated, neutral state and the other with H95 in its doubly protonated, positively charged state. For the neutral state, H95 was protonated in the delta nitrogen of the imidazole ring as predicted by the WHAT IF package. The simulations showed increased water permeability with the doubly protonated H95 residue (H95+) (compare 1.72 ± 0.26 × 10^{-14} cm^3/s with 2.62 ± 0.37 × 10^{-14} cm^3/s, n = 8, p < 0.038) (Figure 2A). To assess if this change was brought about through a purely steric alteration in the pore radius of the monomer, we calculated the radius profile for the channel (Figure 2B). The profile for the AQP4 channel with H95+ was observed to offer a slightly wider pore in the region where the H95 is located. However, this difference was within the SD in the radius as estimated from the trajectory (Figure 2B). This indicated that the change in protonation of the residue did not
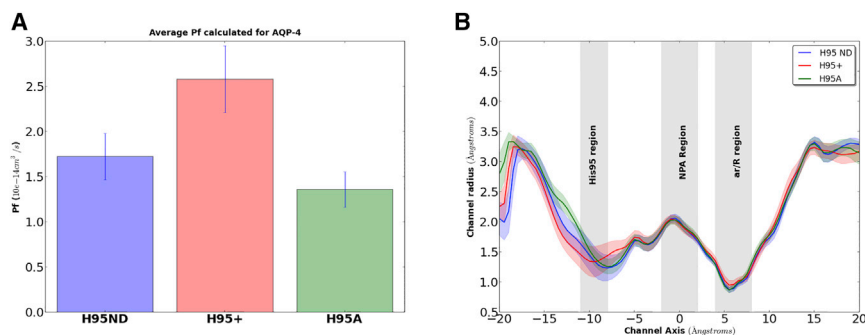
(A) The permeability values (Pf) calculated in the H95 singly protonated simulation are compared with those calculated from the H95+ and H95A simulations.

(B) The profile of the radius along the channel lumen is plotted for comparison between the three simulations. The uncertainty is estimated with the SD calculated in the trajectory.

significantly alter the channel profile in a static manner. Interestingly, the H95 region in the channel profile demonstrated the highest variability in the pore radius. This furthered the possibility of a gating-like behavior in the general vicinity of H95, which could potentially modulate permeability of the monomer channel. As permeability is affected by the protonation state, a pH-dependent gating mechanism was hypothesized.

We used the partial least-squares-based functional mode analysis (PLS-FMA) (Krivobokova et al., 2012) methodology that allows us to capture collective motions in the protein that correlate most with the function of interest. In this case, the local change in the pore radius was used to train the PLS-FMA model. We used the set of local radii in eight non-overlapping regions (Figure 3A) in the channel as a function to train the algorithm. Using this training set with PLS-FMA, we detected eight modes in the simulation system that could potentially explain opening and closing of the channel pore in a local region for the simulation window. PLS-FMA modes with a high cross-validation correlation coefficient ($R^2 > 0.75$) were considered for further investigation.

Of the eight modes obtained through this method, three modes, obtained from the -16 to -8 Å region, the -12 to -8 Å region, and the -8 to -4 Å region, demonstrated the ability to open and close an AQP4 channel significantly by allowing the radius to vary from a value of 2 to 0.5 Å (Figure 3B). The modes obtained from other regions did not show similarly large fluctuations, implying that a gate-like behavior was absent in these regions. The above three regions were in the vicinity of H95. PLS-FMA mode obtained from the -12 to -8 Å region is numerically and functionally identical to the one obtained from the -8 to -4 Å region. This was expected, as H95 is on the border of these two regions (Figure 3A). Thus, H95 has the potential to affect channel pore radius in either region of the protein, as observed in the simulation. The high correlation coefficient (>0.75) in the training as well as the validation set for both regions indicates a robust identification of the mode that affects the pore radius in the vicinity of H95. The exact type of motion of H95 and the associated loop to move in and out of the channel pore are described in Figure 4. A population histogram of the simulations with neutral H95 showed a predisposition of H95 to remain in the closed state of the channel where the pore radius in the vicinity of H95 is narrow (<1.4 Å, approximately the radius of a water molecule). However, in the simulations with H95+, the channel mostly occupied the open state with a wider pore (Figure 5).

Although the mode identified with the PLS-FMA method correlates with a change in the radius of the pore in the vicinity of H95,

it does not guarantee that the actual function of interest, i.e. permeability, is regulated by the collective motion. To test for a causal relation between radius modulation and water permeability, we carried out essential dynamics (ED) simulations. Here, we trapped the AQP4 monomers in an "open" or a "closed" state. To accomplish this, we chose values +2.1 and -2.0 (Figure 5A) of the projection of the eigenvector, representing the open-close transition in H95 region, which correspond to a wide pore and a narrow pore at the location of H95, respectively (Figure 5B). The ED simulations were then restricted to these values to obtain what we termed open and closed states. In the simulations representing the open state, we observed a significant increase in the permeability ($3.02 \pm 0.55 \times 10^{-14}$ cm³/s, n = 8; ~76% increase compared with equilibrium simulations with H95 in the neutral state). On the other hand, the closed simulations showed a reduced permeability similar to that of the channel with a neutral H95 residue ($1.78 \pm 0.25 \times 10^{-14}$ cm³/s, n = 8; unchanged from equilibrium H95ND simulations) (Figure 5C). This supported the initial assumption that a PLS-FMA mode based on change in the radius profile of the channel could be effectively used to predict the permeability of an AQP4 monomer. In MD simulations of the H95A mutant we observed a slightly reduced water permeability compared with the wild-type singly protonated AQP4 channel, although the difference was not statistically significant (compare $1.72 \pm 0.26 \times 10^{-14}$ cm³/s with $1.35 \pm 0.19 \times 10^{-14}$ cm³/s, n = 8, p = 0.23). The channel profile for H95A shows a smaller pore radius close to the H95A mutation site, similar to that of the wild-type singly protonated AQP4, although the variance in the local radius is smaller. In these simulations, the A95 residue is no longer able to move out of the channel pore, providing a constant steric hindrance in the pathway of the water molecules. The calculated permeabilities are tabulated Table S1.

AQP4 heterologously expressed in *Xenopus laevis* oocytes was subsequently used to determine the effect of pH on the permeability of the channel. Osmotic challenge caused a ~15-fold faster shrinkage of AQP4-expressing oocytes compared with that of native uninjected oocytes (compare $1.85 \pm 0.12 \times 10^{-3}$ cm/s [n = 39] with $0.11 \pm 0.01 \times 10^{-3}$ cm/s [n = 10], p < 0.05; representative traces shown in Figure 6A, left and middle). To determine the effect of acidification of the extracellular fluid on the water permeability of AQP4, two water permeability measurements were obtained in control solution (pH 7.4) to ensure a stable baseline prior to a switch to a test solution with pH 6.0. The water permeability was measured after 10 min in the test solution. The rate of shrinkage of the same
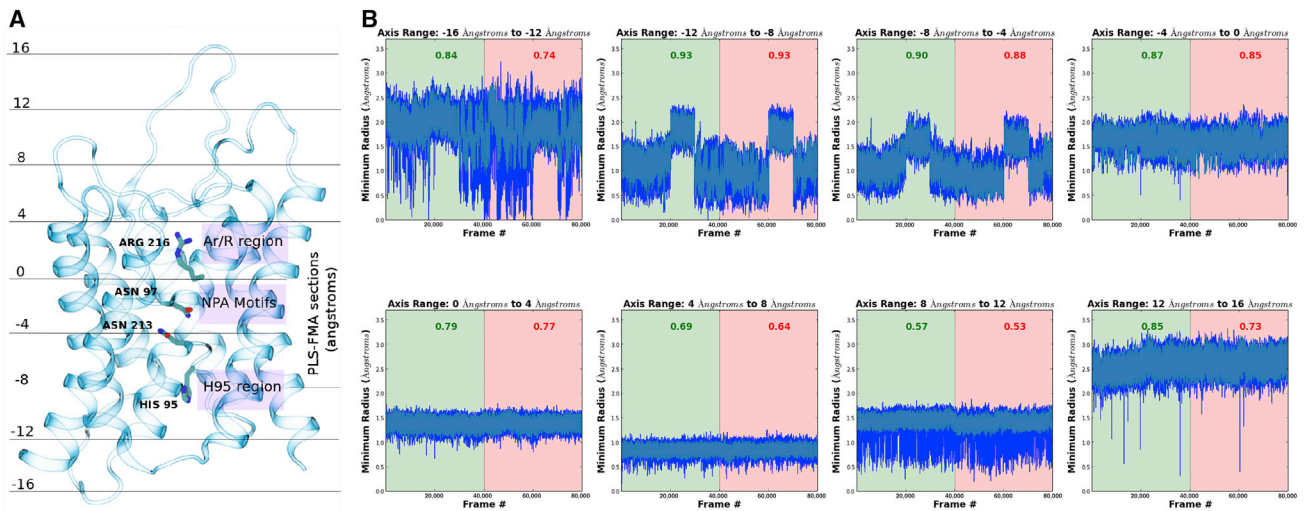
Figure 3. Training and Cross-Validation of the PLS-FMA Model

(A) The AQP4 monomer is divided into eight non-overlapping regions. From each region the lowest value of the radius is drawn to represent each frame and train the PLS-FMA model.

(B) The simulation data are compared with the model generated from the PLS-FMA method. Half of the data (shown on green background) are used for training the model; the remainder (on the red background) are used for cross-validation. The coefficients of regression for the two datasets are shown.

AQP4-expressing oocyte following 10-min exposure to pH 6.0 is illustrated in the right-hand trace of Figure 6A. Figure 6B shows the summarized water permeability of AQP4 at pH 6.0 as a percentage of that obtained at pH 7.4 (102.1% ± 2.1%, n = 22). No significant change in AQP4-induced water permeability was observed upon acidification of the extracellular fluid.

To determine whether AQP4 was sensitive to changes in intracellular pH, the oocyte cytoplasm was acidified by addition of a weak acid (Burckhardt and Frömter, 1992; Stewart et al., 2001) and pH_i was monitored with a H^+-sensitive microelectrode during addition of butyrate to the extracellular solution. A stable pH_i baseline was obtained in control solution prior to exposure of the oocytes to an isosmotic solution containing 40 mM butyrate for 15 min. The course of pH_i is illustrated in Figure 6C, with the addition of butyrate marked with a bar. Butyrate caused an intracellular acidification of both AQP4-expressing (Figure 6C, left trace) and uninjected oocytes (Figure 6C, right trace). Although the AQP4-expressing oocytes had higher basal pH_i than native oocytes (compare 7.34 ± 0.02 [n = 13] with 7.10 ± 0.03 [n = 8], p < 0. 001), addition of butyrate promoted similar acidification in both (compare 6.81 ± 0.03 [n = 13] with 6.73 ± 0.04 [n = 8], p = 0.13, summarized in Figure 6D). Butyrate addition thus caused an acidification of around 0.5 pH units in the AQP4-expressing oocytes. The osmotic water permeability of AQP4-expressing oocytes was determined in control solution (pH 7.4) after which intracellular acidification was obtained by the equimolar replacement of 40 mM NaCl with Na^+-butyrate. The water permeability was measured 10 min after the addition of butyrate. Representative traces of mannitol-induced shrinkage of an AQP4-expressing oocyte before and after 10-min exposure to butyrate are shown in the left panel of Figure 6E. The water permeability of AQP4 increased during intracellular acidification to 111.0% ± 2.2% of control, n = 17, p < 0.001, summarized in Figure 6E, right panel.

To test the role of H95 in the intracellular pH-dependent regulation of AQP4, this residue was mutated to alanine to prevent the pH-induced protonation of the histidine (AQP4.H95A). AQP4.H95A was expressed in oocytes, and the effect of intracellular acidification on the AQP4-mediated osmotic water permeability was evaluated. The rate of shrinkage of an AQP4.H95A-expressing oocyte before and after 10-min exposure to butyrate is shown in Figure 6F, left panel. The water permeability of AQP4.H95A was not significantly changed by intracellular acidification; 98.4% ± 5.2% of control, n = 11, p = 0.76, summarized in the right-hand panel of Figure 6F, underscoring that protonation of H95 does indeed act as the molecular gate, as suggested by the MD simulations.

DISCUSSION

We describe in this work a novel pH-sensitive mechanism to regulate the osmotic water permeability of AQP4. We show that pH changes, mediated by H95, can effectively gate the channel. The H95 residue has a strategic location in the channel, placed at the lumen-bulk interface at the cytosolic side of the AQP4 monomer. This location can expose the H95 to the cytosolic environment of the cell and allow for pH sensitivity. The conservation of this residue across mammalian and plant species also points to the possibility that it might serve a functional purpose. In an earlier work (Janosi and Ceccarelli, 2013), the role of an H95 analog, H67 for AQP5, was proposed to act in a similar manner to modulate the permeability in that protein. Recent work by Alberga et al. (2014) on AQP4 presents a mechanism identifying H95 as the key residue driving the opening and closing of the gating mechanism. However, our investigation reveals that in fact H95 forms the basis for pH-regulated gating. We identify the molecular details involved in this gating and show that the propensity for the "open" state of the channel is strongly influenced by the protonation state of the H95. Several aquaporins
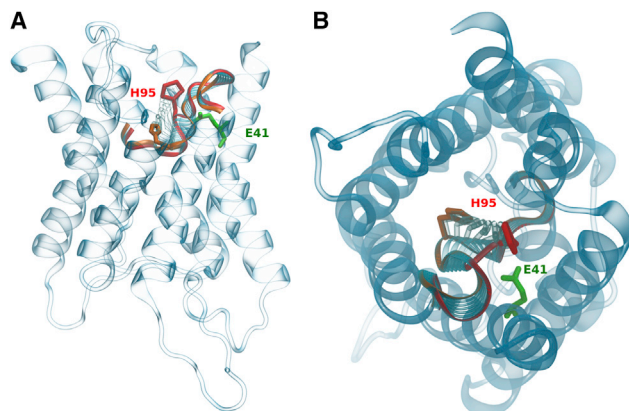
Figure 4. The PLS-FMA Mode Is Shown with the Protein in the Cartoon and the H95 Residue in Licorice Representation

For convenience, the regions of the mode for other parts of the protein are not shown. The extreme closed position of the H95 is shown in orange while the extreme open position is shown in red. The E41 residue, speculated to electrostatically regulate the gate, is shown in green.

(A) The PLS-FMA mode viewed from the side of the monomer.

(B) The PLS-FMA mode, top-down view.

have previously been demonstrated to be regulated by extracellular and/or intracellular pH. Plant AQPs generally appear to decrease their water permeability with decreasing intracellular pH while extracellular pH changes influence mammalian aquaporins in different manners. However, the mechanism proposed in case of plants for the pH regulation of permeability is structurally distinct from the one proposed in this paper (Frick et al., 2013). This mechanism, described for SoPIP2;1, concerns interactions within the loops B and D of the protein to bring about the gating of the channel pore. AQP0 has highest water permeability at pH_e 6.5 (Németh-Cahalan and Hall, 2000), AQP3 closes at pH_e <6 (Zelenina et al., 2003; Zeuthen and Klaerke, 1999), AQP6 opens at pH_e <5.5 (Yasui et al., 1999), whereas AQP4 has been proposed to open at basic pH (Nemeth-Cahalan et al., 2004), a phenomenon we were not able to reproduce in the present study (data not shown).

Herein, a combined experimental and computational investigation strategy was utilized to identify the mechanism by which pH can regulate the water permeability of the AQP4 channel. We use the PLS-FMA methodology to generate collective modes from the simulations that regulate the permeability of the aquaporin. The method can identify concerted motions in proteins that correlate strongly with a function of interest. Functional correlations would not be effectively detected by techniques such as principal component analysis (PCA), as such methods concentrate on identifying collective motions that maximize the covariance. PCA has been proved useful in earlier studies to identify collective modes that are relevant for functioning of the proteins of interest (Autore et al., 2010; Linder et al., 2013). Such a treatment can potentially miss the collective mode of interest if it does not contribute largely to the covariance. Ideally, the training function for the PLS-FMA model in this case would be the osmotic permeability. However, as the permeability of the AQP4 channel appears to have a long autocorrelation time on the order of nanoseconds, we could not obtain sufficient

data to generate a mode that reliably describes the change in water permeability. Hence, we chose to use radius of the pore as the training function, as it was expected to contribute to the overall mobility of water molecules in the channel, acting as a proxy for permeability. From the results of the simulations we expected to see the pH-sensitive elements to be present on one of the lumen openings of the monomer channel, so that they would effectively detect a pH change in the environment. To assess which side of the protein responded to a pH change, we acidified the two compartments independently and measured the change in AQP4-mediated osmotic water permeability across the cell membrane. The acidification of the extracellular compartment did not induce a significant shift in the permeability. The acidification of the intracellular compartment, however, led to an increase in the measured osmotic water permeability, indicating the presence of the mechanism of pH sensitivity located on the cytosol-facing lumen. As histidine residues have a pK_a close to the physiological pH, we expected them to have a significant role in responding to changes in the bulk hydrogen ion concentration. To check whether this residue could actually affect the osmotic water permeability of AQP4, we built computational models analogous to the experimental system. Using MD simulations performed for these models, we compared the effects of the differential protonation of the H95 residue on the permeability of the AQP4 channel. We found that the simulation findings qualitatively agreed with the experiments with the doubly protonated H95 showing a larger permeability when compared with the simulations with the singly protonated H95. A more direct, quantitative comparison is rendered complicated due to environmental factors that are difficult to control. The most important of these could be that all four H95 residues of all the AQP4 proteins might not be protonated under the empirical conditions, thus yielding a comparatively smaller effect of acidification on the water permeability in the in vitro experiments. Also, in the in vitro studies the pH could be lowered only by a margin of 0.5 pH units. Under conditions of systemic ischemia this drop could potentially be larger, leading to a stronger change in permeability of the protein. Furthermore, we speculate that the reason for the change in the preference of the H95 orientation is in the electrostatic interactions within the protein. The doubly protonated H95 residue is placed in the proximity of a highly conserved glutamic acid residue (E41), which could potentially trap the positively charged H95 in an open position (Figure 4). Such a speculation also explains the gradual and monotonous decrease in the distance between E41 and H95 along the H95 mode in the direction of the gate opening, as shown in Figure S2. This mechanism differs from the one proposed by Alberga et al. (2014), as the latter requires the formation of a hydrogen bond with a C178 residue. Although C178 can act as a potential hydrogen donor, we do not observe it engaging in a hydrogen-bonded interaction in our simulation window of 500 ns. Instead, we find a significant change in the sampling of the "open" and "closed" states of the H95 mode dependent on the protonation state of the H95 residue.

Overall, we report a pH-modulated gate for AQP4 that regulates the osmotic water permeability by modulating the local channel radius. The pore modification calculated in the simulation is significant and can affect the traffic of water molecules through the channel. The pH sensitivity offered by the H95
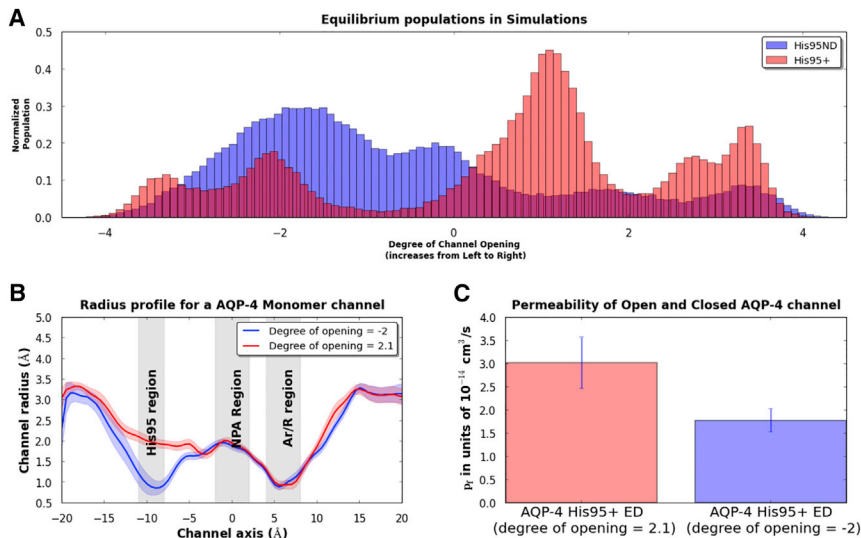
Figure 5. Essential Dynamics Study of the PLS-FMA Mode

(A) The populations of the structures encountered in the equilibrium simulations are plotted as a histogram. The structures are binned against the PLS-FMA vector describing the degree of channel opening in the H95 region. The zero on the x axis approximately equals 1.3 Å radius in the H95 region.

(B) The channel radius profile at two points along the PLS-FMA vector. At a value of −2.0 on the PLS-FMA vector, the channel is constricted at the H95 region, while at the value of +2.1 the local pore near the H95 region appears expanded. These values were then used for the constraints in ED simulations.

(C) The Pf values obtained from the ED simulations are plotted as bar graphs. The "open" ED simulation has a comparatively larger Pf value than the doubly protonated H95 simulation, while the "closed" simulation is reduced to the level of the singly protonated H95 simulation. The uncertainty is estimated from the standard deviation for the Pf values calculated over the four monomer trajectories.

residue combined with its evolutionary conservation points toward a physiological role whereby the channel potentially responds to shifts in the pH in the cytosolic compartment. Thus it can act in a manner that would allow a drop in the cytosolic pH to affect the channel to open wider and, when faced with osmotic pressure, increase the flow of water across the cell membrane. It must be noted that the constriction of the channel at the ar/R region is the narrowest region of the monomer lumen and poses the largest barrier to permeants. This barrier appears to be directly maintained by the physical presence of R216 in the channel pore, which would explain why the radius modulation from the H95 residue cannot completely switch off the channel but regulates the permeability more moderately.

EXPERIMENTAL PROCEDURES

Molecular Dynamics Simulations

The structure used for the simulation of AQP4 was obtained from the PDB (PDB: 3GD8) with a resolution of 1.8 Å (Ho et al., 2009). We used the package WHAT IF (Vriend, 1990) to curate the structure and predict the protonation states of the residues using hydrogen-bond networks. The tetramer generated from this structure was inserted into a lipid bilayer consisting of 294 dimyristoylphosphatidylcholine (DMPC) lipids. This insertion was accomplished with the g_membed tool implementation in GROMACS (Wolf et al., 2010). We used a physiological ion concentration of 150 mM, which was simulated with sodium and chloride ions. The system was maintained at overall neutral charge. The simulation box was solvated with approximately 22,000 explicit water molecules of the SPC/E water model (Berendsen et al., 1987). The electrostatic interactions were simulated explicitly with a cutoff of 1.0 nm using Particle Mesh Ewald (Darden et al., 1993) for long-range interactions. The Lennard-Jones interactions were accounted for with a cutoff of 1.0 nm. All the simulations were carried out using the MD simulations package GROMACS version 4.5.5 (Hess et al., 2008). The LINCS algorithm (Hess, 2008) as implemented in the package was used to constrain the covalent bonds in the system, while the non-polar hydrogens were replaced with v-sites (Feenstra et al., 1999). v-Sites allowed us to reach a time step of 4 fs. The simulations were performed at a temperature of 300 K using a velocity-rescale thermostat (Bussi et al., 2007) and at 1 atm pressure maintained by the Parrinello-Rahman barostat. The DMPC lipids were simulated with Berger parameters (Berger et al., 1997). The parameters for the protein and the ions

were obtained from the AMBER99SB-ILDN force field (Hornak et al., 2006; Lindorff-Larsen et al., 2010). DMPC lipids were chosen for several reasons. These lipids do not pose a significant hydrophobic mismatch with the protein. Earlier, they have been used to reproduce physiological arrangements and permeabilities for AQP0 (Gonen et al., 2005). Also, MD simulation results agree with experiments within this and previous work.

Two equilibrium simulations of 500 ns each were performed to study the effect of varying protonation states of H95 on the permeability of the channel. To calculate the permeability, we used the collective diffusion method as described by Zhu et al. (2004). We assumed that the four monomers of the AQP4 channel were not correlated in terms of their permeability. This allowed us to use every monomer as an independent channel to yield four-fold statistics. We discarded the first 100 ns of simulation trajectory to account for equilibration. To calculate the average permeability, we divided the remaining simulation trajectory into eight equal sections of 50 ns each. For each monomer, the average was computed over the four monomers. The SE over the eight sections was then used to estimate the uncertainty in the permeability. The package HOLE was used to calculate the radius profile of the AQP4 monomer channel (Smart et al., 1993). The conservation within sequences of aquaporins was studied with the web-plugin JalView (Waterhouse et al., 2009). A snapshot of the simulation system is shown in Figure S1.

Functional Mode Analysis

To identify the collective mode that correlates best with the opening and closing transitions of the channel protein, we used FMA (Hub and de Groot, 2009) based on the machine-learning algorithm PLS fitting, as implemented for computational molecular simulations (Krivobokova et al., 2012). We divided the monomer channel axis into eight equally spaced regions along its length. From each of these regions, we calculated the smallest radius for every frame in the equilibrium trajectory, creating eight data vectors. Each data vector was used as a function to generate one PLS-FMA model corresponding to the local change in channel radius. Only half of the data from the data vectors were used for training the models; the rest were used for cross-validation. This allowed us to correct for any possible overfitting in the process of model generation. The number of components used to create a model was varied from 1 to 25 to compare the cross-validation correlation coefficients. For the final analysis, the model with 15 components was chosen.

Essential Dynamics Simulations

To validate the causal effect of the collective mode predicted by the PLS-FMA methodology on channel opening, ED simulations were performed as implemented in the GROMACS package (Amadei et al., 1993, 1996). These
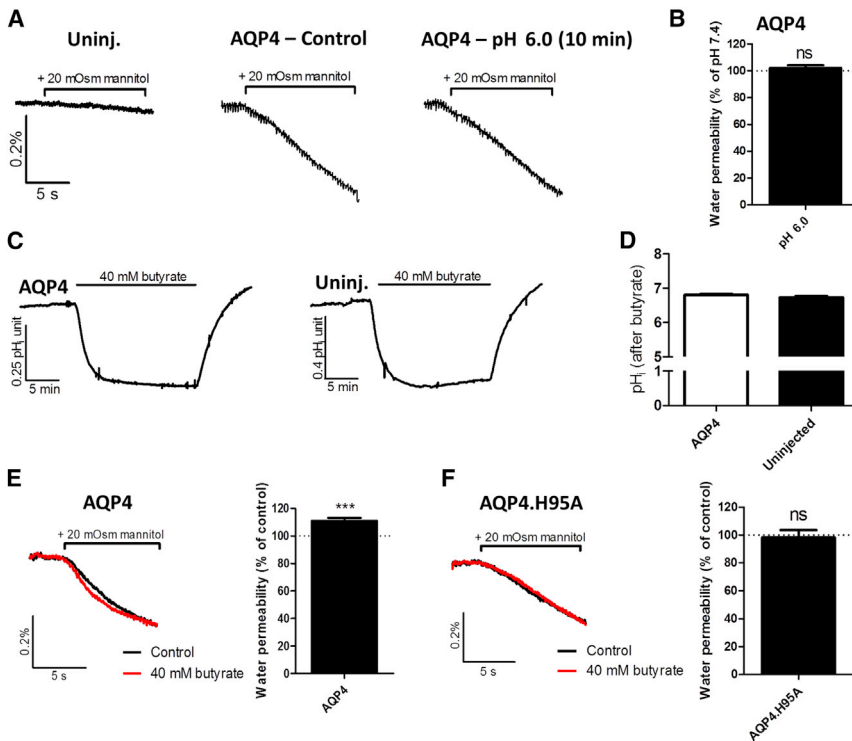
Figure 6. pH Dependence of AQP4 Expressed in *Xenopus* Oocytes

(A) Volume traces from an uninjected oocyte (left trace) and an AQP4-expressing oocyte (middle trace) challenged with a hyperosmotic gradient of 20 mOsm as indicated by the bar, at pH 7.4. The same AQP4-expressing oocyte was subsequently challenged with a hyperosmotic gradient during exposure to extracellular acidification (pH 6.0) for 10 min (right trace).

(B) Summarized water permeabilities of AQP4-expressing oocytes after 10-min exposure to extracellular acidification (pH 6.0) relative to control measurements; n = 22. Paired t test was not significant (ns).

(C) pH$_i$ traces from an AQP4-expressing (left trace) and uninjected (right trace) oocyte during exposure to 40 mM butyrate (indicated by bar) for 15 min.

(D) Summarized pH$_i$ after 10-min exposure to 40 mM butyrate of AQP4-expressing (n = 13) and uninjected (n = 8) oocytes.

(E) Left: Volume traces from an AQP4-expressing oocyte challenged with a hyperosmotic gradient before (black) and after exposure to intracellular acidification with 40 mM butyrate (red) for 10 min. Right: Summarized water permeabilities of AQP4-expressing oocytes after 10-min exposure of 40 mM butyrate relative to control measurements; n = 17. Paired t test: ***p < 0.001.

(F) Left: Volume traces from an AQP4.H95A-expressing oocyte challenged with a hyperosmotic gradient before (black) and after exposure to intracellular acidification with 40 mM butyrate (red) for 10 min. Right: Summarized water permeabilities of AQP4-expressing oocytes after 10-min exposure of 40 mM butyrate relative to control measurements; n = 11. Paired t test: not significant (ns).

simulations tested the ability of the PLS-FMA mode to regulate the permeability of the AQP4 water channel. In the first simulation, all four monomer channels were trapped in the "open" configuration of the mode, and in the second simulation they were all confined to the "closed" configuration of the same mode. Here open and closed refer respectively to configurations with a large and a small pore radius in the vicinity of the H95 residue. The ability of a configuration to restrict the channel in an open or closed form was tested by calculating the pore profile with the HOLE package. This restriction was achieved with a force constant of 1,000 kJ mol^{-1} nm^{-1}. These configurations were obtained by imposing restraints on protein dynamics along projections of the eigenvector maximizing the covariance in the PLS-FMA mode. Both of these simulations were carried out for 100 ns, and the first 10 ns were dropped to account for equilibration in subsequent analysis. The permeability was calculated with the same method previously used for equilibrium simulations. SD in the permeability was used to calculate uncertainty in the measurement.

Oocyte Preparation

X. laevis frogs were obtained from Nasco or *Xenopus* Express. Oocytes were surgically removed from anesthetized frogs, and the follicular membrane was removed by collagenase treatment (Type 1, Worthington Biochemical or collagenase A, Roche) as previously described (Becker and Deitmer, 2004; Fenton et al., 2010). The singularized oocytes were left overnight in Kulori medium (90 mM NaCl, 1 mM KCl, 1 mM CaCl$_2$, 1 mM MgCl$_2$, 5 mM HEPES [pH 7.4–7.8]) at 18°C to recover. The protocol complies with the European Community guidelines for the use of experimental animals and the experiments were approved by The Danish National Committee for Animal Studies or by The Landesuntersuchungsamt Rheinland-Pfalz, Koblenz.

Molecular Biology

Mutations in AQP4 were introduced into wild-type rat AQP4.M23 (Lu et al., 1996) subcloned into the oocyte expression vector pXOOM, using a Quick Change site-directed mutagenesis kit (Stratagene), and verified with DNA sequencing. Numbering of the AQP4 amino acids is in accord with that of

AQP4.M1. The cDNAs encoding the AQP4 constructs were linearized downstream of the poly(A) segment and in vitro transcribed using T7 mMessage Machine (Ambion). cRNA was extracted with MEGAclear (Ambion), and microinjected into defolliculated *X. laevis* oocytes of stages V and VI (25 ng/oocyte). Oocytes were incubated in Kulori medium for 3–4 days at 18°C–19°C prior to experiments.

Oocyte Volume Measurements

The experimental setup for measuring water permeability of oocytes has been described in detail previously (Zeuthen et al., 2006). The oocyte was perfused with a control solution (100 mM NaCl, 2 mM KCl, 1 mM CaCl$_2$, 1 mM MgCl$_2$, 10 mM HEPES [pH 7.4]) and subsequently one of two test solutions (100 mM NaCl, 2 mM KCl, 1 mM CaCl$_2$, 1 mM MgCl$_2$, 10 mM HEPES [pH 6.0]; or 60 mM NaCl, 40 mM Na-butyrate, 2 mM KCl, 1 mM CaCl$_2$, 1 mM MgCl$_2$, 10 mM HEPES [pH 7.4]) at room temperature (21°C–24°C) in a small chamber with a glass bottom. The oocyte was viewed from below via a long-distance objective, and oocyte images were captured continuously at a rate of 25 images/s. To determine the water permeability, the oocytes were abruptly challenged with a hypertonic solution (control or test solution with additional 20 mOsm mannitol), and the water permeability was calculated as

$$L_p = \frac{-J_v}{A \cdot \Delta\pi \cdot V_w} ,$$

where J_v is the water flux during the osmotic challenge, A is the true membrane surface area (about nine times the apparent area due to membrane folding [Zampighi et al., 1995]), $\Delta\pi$ is the osmotic challenge, V_w is the partial molal volume of water, i.e. 18 cm^3/mol, and L_p is the water permeability given in units of cm/s. The osmotic water permeability of AQP4-expressing oocytes was determined in control solution by double determination, and the water permeability of uninjected oocytes was subtracted.

Intracellular pH Measurements

Changes in intracellular pH (pH$_i$) in oocytes were determined with ion-selective microelectrodes under voltage-clamp conditions. For measurement of

intracellular pH and membrane potential, double-barreled microelectrodes were used; the manufacture and application have been described in detail previously (Deitmer, 1991). For calibration, electrodes were perfused with HEPES-buffered control solution (100 mM NaCl, 2 mM KCl, 1 mM CaCl$_2$, 1 mM MgCl$_2$, 10 mM HEPES [pH 7.4]) and, after a stable electrode potential was reached, control solution pH 7.0 was applied until the electrode again reached a stable potential. The subsequent measurements of oocyte pH$_i$ were stored digitally using home-made PC software based on the program LabView (National Instruments Germany). For two-electrode voltage clamp, a borosilicate glass capillary, 1.5 mm in diameter, was pulled to a micropipette and backfilled with 3 M KCl. This electrode was used for current injection and was connected to the head-stage of an Axoclamp 2A amplifier (Axon Instruments). The actual membrane voltage was recorded by the reference barrel of the double-barreled pH-sensitive microelectrode. Oocytes were clamped to a holding potential of −40 mV. As described previously (Bröer et al., 1998), optimal intracellular pH changes were detected when the ion-selective electrode was located near the inner surface of the plasma membrane. All experiments were carried out at room temperature 3–6 days after injection of cRNA into the oocytes.

SUPPLEMENTAL INFORMATION

Supplemental Information includes two figures and one table and can be found with this article online at http://dx.doi.org/10.1016/j.str.2015.08.020.

ACKNOWLEDGMENTS

REFERENCES

Agre, P. (2006). The aquaporin water channels. Proc. Am. Thorac. Soc. 3, 5–13.

Agre, P., King, L.S., Yasui, M., Guggino, W.B., Ottersen, O.P., Fujiyoshi, Y., Engel, A., and Nielsen, S. (2002). Aquaporin water channels—from atomic structure to clinical medicine. J. Physiol. 542, 3–16.

Alberga, D., Nicolotti, O., Lattanzi, G., Nicchia, G.P., Frigeri, A., Pisani, F., Benfenati, V., and Mangiatordi, G.F. (2014). A new gating site in human aquaporin-4: insights from molecular dynamics simulations. Biochim. Biophys. Acta 1838, 3052–3060.

Amadei, A., Linssen, A.B.M., and Berendsen, H.J.C. (1993). Essential dynamics of proteins. Proteins 17, 412–425.

Amadei, A., Linssen, A.B.M., de Groot, B.L., van Aalten, D.M.F., and Berendsen, H.J.C. (1996). An efficient method for sampling the essential subspace of proteins. J. Biomol. Struct. Dyn. 13, 615–625.

Amiry-Moghaddam, M., and Ottersen, O.P. (2003). The molecular basis of water transport in the brain. Nat. Rev. Neurosci. 4, 991–1001.

Assentoft, M., Kaptan, S., Fenton, R.A., Hua, S.Z., de Groot, B.L., and MacAulay, N. (2013). Phosphorylation of rat aquaporin-4 at Ser111 is not required for channel gating. Glia 61, 1101–1112.

Assentoft, M., Larsen, B.R., Olesen, E.T., Fenton, R.A., and MacAulay, N. (2014). AQP4 plasma membrane trafficking or channel gating is not significantly modulated by phosphorylation at COOH-terminal serine residues. Am J Physiol Cell Physiol. 307 (10), C957–965.

Autore, F., Pagano, B., Fornili, A., Rittinger, K., and Fraternali, F. (2010). In silico phosphorylation of the autoinhibited form of p47phox: insights into the mechanism of activation. Biophys. J. 99, 3716–3725.

Becker, H.M., and Deitmer, J.W. (2004). Voltage dependence of H$^+$ buffering mediated by sodium bicarbonate cotransport expressed in Xenopus oocytes. J. Biol. Chem. 279, 28057–28062.

Beitz, E., Pavlovic-Djuranovic, S., Yasui, M., Agre, P., and Schultz, J.E. (2004). Molecular dissection of water and glycerol permeability of the aquaglyceroporin from Plasmodium falciparum by mutational analysis. Proc. Natl. Acad. Sci. USA 101, 1153–1158.

Beppu, K., Sasaki, T., Tanaka, K.F., Yamanaka, A., Fukazawa, Y., Shigemoto, R., and Matsui, K. (2014). Optogenetic countering of glial acidosis suppresses glial glutamate release and ischemic brain damage. Neuron 81, 314–320.

Berendsen, H.J.C., Grigera, J.R., and Straatsma, T.P. (1987). The missing term in effective pair potentials. J. Phys. Chem. 91, 6269–6271.

Berger, O., Edholm, O., and Jahnig, F. (1997). Molecular dynamics simulations of a fluid bilayer of dipalmitoylphosphatidylcholine at full hydration, constant pressure, and constant temperature. Biophys. J. 72, 2002–2013.

Bröer, S., Schneider, H.P., Bröer, A., Rahman, B., Hamprecht, B., and Deitmer, J.W. (1998). Characterization of the monocarboxylate transporter 1 expressed in Xenopus laevis oocytes by changes in cytosolic pH. Biochem. J. 333, 167–174.

Burckhardt, B.C., and Frömter, E. (1992). Pathways of NH3/NH4+ permeation across Xenopus laevis oocyte cell membrane. Pflugers Arch. 420, 83–86.

Burykin, A., and Warshel, A. (2004). On the origin of the electrostatic barrier for proton transport in aquaporin. FEBS Lett. 570, 41–46.

Bussi, G., Donadio, D., and Parrinello, M. (2007). Canonical sampling through velocity rescaling. J. Chem. Phys. 126, 014101.

Cooper, G.J., Zhou, Y., Bouyer, P., Grichtchenko, I.I., and Boron, W.F. (2002). Transport of volatile solutes through AQP1. J. Physiol. 542, 17–29.

Cui, Y., and Bastien, D.A. (2011). Water transport in human aquaporin-4: molecular dynamics (MD) simulations. Biochem. Biophys. Res. Commun. 412, 654–659.

Darden, T., York, D., and Pedersen, L. (1993). Particle mesh Ewald: an N·log(N) method for Ewald sums in large systems. J. Chem. Phys. 98, 10089–10092.

de Groot, B.L., and Grubmüller, H. (2001). Water permeation across biological membranes: mechanism and dynamics of aquaporin-1 and GlpF. Science 294, 2353–2357.

de Groot, B.L., and Grubmüller, H. (2005). The dynamics and energetics of water permeation and proton exclusion in aquaporins. Curr. Opin. Struct. Biol. 15, 176–183.

de Groot, B.L., Frigato, T., Helms, V., and Grubmüller, H. (2003). The mechanism of proton exclusion in the aquaporin-1 water channel. J. Mol. Biol. 333, 279–293.

Deitmer, J.W. (1991). Electrogenic sodium-dependent bicarbonate secretion by glial cells of the leech central nervous system. J. Gen. Physiol. 98, 637–655.

Endeward, V., Musa-Aziz, R., Cooper, G.J., Chen, L.-M., Pelletier, M.F., Virkki, L.V., Supuran, C.T., King, L.S., Boron, W.F., and Gros, G. (2006). Evidence that aquaporin 1 is a major pathway for CO$_2$ transport across the human erythrocyte membrane. FASEB J. 20, 1974–1981.

Feenstra, K.A., Hess, B., and Berendsen, H.J.C. (1999). Improving efficiency of large time-scale molecular dynamics simulations of hydrogen-rich systems. J. Comput. Chem. 20, 786–798.

Fenton, R.A., Moeller, H.B., Zelenina, M., Snaebjornsson, M.T., Holen, T., and MacAulay, N. (2010). Differential water permeability and regulation of three aquaporin 4 isoforms. Cell Mol. Life Sci. 67, 829–840.

Frick, A., Järvå, M., and Törnroth-Horsefield, S. (2013). Structural basis for pH gating of plant aquaporins. FEBS Lett. 587, 989–993.

Frick, A., Eriksson, U.K., de Mattia, F., Oberg, F., Hedfalk, K., Neutze, R., de Grip, W.J., Deen, P.M.T., and Törnroth-Horsefield, S. (2014). X-Ray structure of human aquaporin 2 and its implications for nephrogenic diabetes insipidus and trafficking. Proc. Natl. Acad. Sci. USA 111, 6305–6310.

Fu, D., Libson, A., Miercke, L.J.W., Weitzman, C., Nollert, P., Krucinski, J., and Stroud, R.M. (2000). Structure of a glycerol-conducting channel and the basis for its selectivity. Science *290*, 481–486.

Garate, J.-A., English, N.J., and MacElroy, J.M.D. (2011). Human aquaporin 4 gating dynamics in dc and ac electric fields: a molecular dynamics study. J. Chem. Phys. *134*, 055110.

Gonen, T., Cheng, Y., Sliz, P., Hiroaki, Y., Fujiyoshi, Y., Harrison, S.C., and Walz, T. (2005). Lipid–protein interactions in double-layered two-dimensional AQP0 crystals. Nature *438*, 633–638.

Gunnarson, E., Zelenina, M., Axehult, G., Song, Y., Bondar, A., Krieger, P., Brismar, H., Zelenin, S., and Aperia, A. (2008). Identification of a molecular target for glutamate regulation of astrocyte water permeability. Glia *56*, 587–596.

Harries, W.E.C., Akhavan, D., Miercke, L.J.W., Khademi, S., and Stroud, R.M. (2004). The channel architecture of aquaporin 0 at a 2.2-Å resolution. Proc. Natl. Acad. Sci. USA *101*, 14045–14050.

Hess, B. (2008). P-LINCS: a parallel linear constraint solver for molecular simulation. J. Chem. Theor. Comput. *4*, 116–122.

Hess, B., Kutzner, C., van der Spoel, D., and Lindahl, E. (2008). GROMACS 4: algorithms for highly efficient, load-balanced, and scalable molecular simulation. J. Chem. Theor. Comput. *4*, 435–447.

Heymann, J.B., and Engel, A. (1999). Aquaporins: phylogeny, structure, and physiology of water channels. News Physiol. Sci. *14*, 187–193.

Ho, J.D., Yeh, R., Sandstrom, A., Chorny, I., Harries, W.E.C., Robbins, R.A., Miercke, L.J.W., and Stroud, R.M. (2009). Crystal structure of human aquaporin 4 at 1.8 Å and its mechanism of conductance. Proc. Natl. Acad. Sci. USA *106*, 7437–7442.

Hornak, V., Abel, R., Okur, A., Strockbine, B., Roitberg, A., and Simmerling, C. (2006). Comparison of multiple Amber force fields and development of improved protein backbone parameters. Proteins *65*, 712–725.

Horsefield, R., Nordén, K., Fellert, M., Backmark, A., Törnroth-Horsefield, S., Scheltinga, A.C.T.v., Kvassman, J., Kjellbom, P., Johanson, U., and Neutze, R. (2008). High-resolution x-ray structure of human aquaporin 5. Proc. Natl. Acad. Sci. USA *105*, 13327–13332.

Hub, J.S., and de Groot, B.L. (2008). Mechanism of selectivity in aquaporins and aquaglyceroporins. Proc. Natl. Acad. Sci. USA *105*, 1198–1203.

Hub, J.S., and de Groot, B.L. (2009). Detection of functional modes in protein dynamics. PLoS Comput. Biol. *5*, e1000480.

Hub, J.S., Grubmüller, H., and de Groot, B.L. (2009). Dynamics and energetics of permeation through aquaporins. What do we learn from molecular dynamics simulations? Handb. Exp. Pharmacol. *190*, 57–76.

Janosi, L., and Ceccarelli, M. (2013). The gating mechanism of the human aquaporin 5 revealed by molecular dynamics simulations. PLoS One *8*, e59897.

Kraig, R.P., and Chesler, M. (1990). Astrocytic acidosis in hyperglycemic and complete ischemia. J. Cereb. Blood Flow Metab. *10*, 104–114.

Krivobokova, T., Briones, R., Hub, J.S., Munk, A., and de Groot, B.L. (2012). Partial least-squares functional mode analysis: application to the membrane proteins AQP1, Aqy1, and CLC-ec1. Biophys. J. *103*, 786–796.

Lascola, C., and Kraig, R.P. (1997). Astroglial acid-base dynamics in hyperglycemic and normoglycemic global ischemia. Neurosci. Biobehav. Rev. *21*, 143–150.

Lee, J.K., Kozono, D., Remis, J., Kitagawa, Y., Agre, P., and Stroud, R.M. (2005). Structural basis for conductance by the archaeal aquaporin AqpM at 1.68 Å. Proc. Natl. Acad. Sci. USA *102*, 18932–18937.

Lin, Y., Cao, Z., and Mo, Y. (2006). Molecular dynamics simulations on the *Escherichia coli* ammonia channel protein AmtB: mechanism of ammonia/ammonium transport. J. Am. Chem. Soc. *128*, 10876–10884.

Linder, T., de Groot, B.L., and Stary-Weinzinger, A. (2013). Probing the energy landscape of activation gating of the bacterial potassium channel KcsA. PLoS Comput. Biol. *9*, e1003058.

Lindorff-Larsen, K., Piana, S., Palmo, K., Maragakis, P., Klepeis, J.L., Dror, R.O., and Shaw, D.E. (2010). Improved side-chain torsion potentials for the Amber ff99SB protein force field. Proteins *78*, 1950–1958.

Lu, M., Lee, M.D., Smith, B.L., Jung, J.S., Agre, P., Verdijk, M.A., Merkx, G., Rijss, J.P., and Deen, P.M. (1996). The human AQP4 gene: definition of the locus encoding two water channel polypeptides in brain. Proc. Natl. Acad. Sci. USA *93*, 10908–10912.

Meinild, A.K., Klaerke, D.A., and Zeuthen, T. (1998). Bidirectional water fluxes and specificity for small hydrophilic molecules in aquaporins 0–5. J. Biol. Chem. *273*, 32446–32451.

Murata, K., Mitsuoka, K., Hirai, T., Walz, T., Agre, P., Heymann, J.B., Engel, A., and Fujiyoshi, Y. (2000). Structural determinants of water permeation through aquaporin-1. Nature *407*, 599–605.

Németh-Cahalan, K.L., and Hall, J.E. (2000). pH and calcium regulate the water permeability of aquaporin 0. J. Biol. Chem. *275*, 6777–6782.

Nemeth-Cahalan, K.L., Kalman, K., and Hall, J.E. (2004). Molecular basis of pH and Ca^{2+} regulation of aquaporin water permeability. J. Gen. Physiol. *123*, 573–580.

Newby, Z.E.R., O'Connell Iii, J., Robles-Colmenares, Y., Khademi, S., Miercke, L.J., and Stroud, R.M. (2008). Crystal structure of the aquaglyceroporin PfAQP from the malarial parasite Plasmodium falciparum. Nat. Struct. Mol. Biol. *15*, 619–625.

Nielsen, S., Nagelhus, E.A., Amiry-Moghaddam, M., Bourque, C., Agre, P., and Ottersen, O.P. (1997). Specialized membrane domains for water transport in glial cells: high-resolution immunogold cytochemistry of aquaporin-4 in rat brain. J. Neurosci. *17*, 171–180.

Reale, R., English, N.J., Garate, J.-A., Marracino, P., Liberti, M., and Apollonio, F. (2013). Human aquaporin 4 gating dynamics under and after nanosecond-scale static and alternating electric-field impulses: a molecular dynamics study of field effects and relaxation. J. Chem. Phys. *139*, 205101.

Ringel, F., Chang, R.C., Staub, F., Baethmann, A., and Plesnila, N. (2000). Contribution of anion transporters to the acidosis-induced swelling and intracellular acidification of glial cells. J. Neurochem. *75*, 125–132.

Sachdeva, R., and Singh, B. (2014a). Insights into structural mechanisms of gating induced regulation of aquaporins. Prog. Biophys. Mol. Biol. *114*, 69–79.

Sachdeva, R., and Singh, B. (2014b). Phosphorylation of Ser-180 of rat aquaporin-4 shows marginal affect on regulation of water permeability: molecular dynamics study. J. Biomol. Struct. Dyn. *32*, 555–566.

Savage, D.F., Egea, P.F., Robles-Colmenares, Y., O'Connell, J.D., and Stroud, R.M. (2003). Architecture and selectivity in aquaporins: 2.5 Å X-ray structure of aquaporin Z. PLoS Biol. *1*, E72.

Smart, O.S., Goodfellow, J.M., and Wallace, B.A. (1993). The pore dimensions of gramicidin A. Biophys. J. *65*, 2455–2460.

Stewart, A.K., Chernova, M.N., Kunes, Y.Z., and Alper, S.L. (2001). Regulation of AE2 anion exchanger by intracellular pH: critical regions of the NH(2)-terminal cytoplasmic domain. Am. J. Physiol. Cell Physiol. *281*, C1344–C1354.

Sui, H., Han, B.-G., Lee, J.K., Walian, P., and Jap, B.K. (2001). Structural basis of water-specific transport through the AQP1 water channel. Nature *414*, 872–878.

Törnroth-Horsefield, S., Wang, Y., Hedfalk, K., Johanson, U., Karlsson, M., Tajkhorshid, E., Neutze, R., and Kjellbom, P. (2006). Structural mechanism of plant aquaporin gating. Nature *439*, 688–694.

Verkman, A.S. (2002). Does aquaporin-1 pass gas? An opposing view. J. Physiol. *542*, 31.

Vriend, G. (1990). WHAT IF: a molecular modeling and drug design program. J. Mol. Graph. *8*, 52–56.

Wang, Y., and Tajkhorshid, E. (2010). Nitric oxide conduction by the brain aquaporin AQP4. Proteins *78*, 661–670.

Waterhouse, A.M., Procter, J.B., Martin, D.M.A., Clamp, M., and Barton, G.J. (2009). Jalview version 2—a multiple sequence alignment editor and analysis workbench. Bioinformatics *25*, 1189–1191.

Wolf, M.G., Hoefling, M., Aponte-Santamaría, C., Grubmüller, H., and Groenhof, G. (2010). g_membed: efficient insertion of a membrane protein

into an equilibrated lipid bilayer with minimal perturbation. J. Comput. Chem. *31*, 2169–2174.

Yasui, M., Hazama, A., Kwon, T.H., Nielsen, S., Guggino, W.B., and Agre, P. (1999). Rapid gating and anion permeability of an intracellular aquaporin. Nature *402*, 184–187.

Yu, J., Yool, A.J., Schulten, K., and Tajkhorshid, E. (2006). Mechanism of gating and ion conductivity of a possible tetrameric pore in Aquaporin-1. Structure *14*, 1411–1423.

Zador, Z., Stiver, S., Wang, V., and Manley, G.T. (2009). Role of aquaporin-4 in cerebral edema and stroke. Handb. Exp. Pharmacol. *190*, 159–170.

Zampighi, G.A., Kreman, M., Boorer, K.J., Loo, D.D., Bezanilla, F., Chandy, G., Hall, J.E., and Wright, E.M. (1995). A method for determining the unitary functional capacity of cloned channels and transporters expressed in *Xenopus laevis* oocytes. J. Membr. Biol. *148*, 65–78.

Zelenina, M., Zelenin, S., Bondar, A.A., Brismar, H., and Aperia, A. (2002). Water permeability of aquaporin 4 is decreased by protein kinase C and dopamine. Am. J. Physiol. Renal Physiol. *283*, F309–F318.

Zelenina, M., Bondar, A.A., Zelenin, S., and Aperia, A. (2003). Nickel and extracellular acidification inhibit the water permeability of human aquaporin-3 in lung epithelial cells. J. Biol. Chem. *278*, 30037–30043.

Zeuthen, T., and Klaerke, D.A. (1999). Transport of water and glycerol in aquaporin 3 is gated by H$^+$. J. Biol. Chem. *274*, 21631–21636.

Zeuthen, T., Belhage, B., and Zeuthen, E. (2006). Water transport by Na+-coupled cotransporters of glucose (SGLT1) and of iodide (NIS). The dependence of substrate size studied at high resolution. J. Physiol. *570*, 485–499.

Zhu, F., Tajkhorshid, E., and Schulten, K. (2004). Collective diffusion model for water permeation through microscopic channels. Phys. Rev. Lett. *93*, 224501.